Mon. Not. R. astr. Soc. (1975) **173**, 671–699.

MODELS FOR THE FORMATION OF ELLIPTICAL GALAXIES

Richard B. Larson

Yale University Observatory, New Haven, Connecticut 06520

(Received 1975 June 3; in original form 1975 May 6)

SUMMARY

Previous models for the formation and evolution of spherical galaxies are here generalized to the case of axisymmetric rotating systems. It is found that a completely inviscid collapse does not yield a realistic model, but if a plausible turbulent viscosity is assumed it produces significant outward transfer of angular momentum during the collapse and leads to models which closely resemble elliptical galaxies. The radial structure of these models is similar to that of the spherical models, but the rotating models also predict isophotal shapes, ellipticity profiles, and rotation curves that are in qualitative agreement with observations. The distributions of metal abundance, rotational velocity, and velocity dispersion are all flattened toward the equatorial plane, and reflect a stellar population gradient perpendicular to this plane which is qualitatively similar to the stellar population gradient observed in our galaxy. If there is not too much viscosity present during the later stages of the collapse, the residual gas forms a distinct flat 'incipient disc' component.

1. INTRODUCTION

In two two previous papers (Larson 1969, Paper I; Larson 1974a, Paper II) results were presented for a number of dynamical calculations describing the formation and evolution of spherical galaxies. In these papers it was shown that when plausible values are assumed for the model parameters these spherical models reproduce the radial surface brightness profiles of typical elliptical galaxies, as well as the observed metal abundance gradients. However, in view of the fact that most, if not all, elliptical galaxies rotate and have finite flattening (de Vaucouleurs 1974), it would clearly be desirable to undertake similar calculations also for flattened rotating models. The additional properties of elliptical galaxies which one might hope to be able to explain with such models include the rotation curves, isophotal shapes, and ellipticity profiles; also, as more observational data become available, it will be useful to have predictions for the complete two-dimensional distributions of metal abundance and kinematic properties over the image of an elliptical galaxy. In the present paper we describe a number of calculations of axisymmetric rotating models intended to represent more realistically the structure of rotating elliptical galaxies. Calculations for more highly-flattened models with prominent disc components are in progress and will be reported in a later paper.

In Papers I and II it was assumed that a protogalaxy begins as a cloud of gas, and that star formation takes place continuously during the collapse of the protogalaxy; a two-fluid hydrodynamic treatment was then used to describe the

dynamics of the system of both gas and stars. Rather different assumptions have been made in the recent work of Gott (1973, 1975), who has calculated models for the formation of elliptical galaxies on the assumption that star formation is completed before the collapse begins, so that only the dynamics of a system of stars need be considered. When 'cosmological infall' effects are included (Gott 1975) these purely stellar models are able to reproduce the observed flattening and the brightness profiles of the envelopes of elliptical galaxies, but the dense nuclei observed in many E galaxies are not reproduced, nor are the metal abundance gradients. To explain these properties, it still appears necessary to assume that at least the inner parts of elliptical galaxies have been formed by a gaseous infall process, as in the models of Papers I and II. (For a more complete discussion of models of galaxy formation see Larson 1975.) A gaseous infall model seems especially to be required if, as suggested by recent observations of NGC 3379 by Burkhead & Kalinowski (1974), the composition gradients in E galaxies are not confined to their nuclear regions but extend throughout their envelopes as well; this evidence would suggest that a model such as Model F of Paper II, which predicts a composition gradient at all radii, is preferable to a purely stellar model which predicts no composition gradient.

2. ASSUMPTIONS

2.1 *Initial and boundary conditions*

The present model calculations have all started with a uniform spherical protogalaxy of mass $M = 10^{11} M_{\odot}$ and radius $R = 30$ kpc. As in most of the spherical models of Papers I and II, we have assumed that the boundary remains at a fixed radius and that there is no mass flow across the boundary. It is clear from the previous results for the spherical models that the main effect of assuming a larger boundary radius or an expanding boundary would be to lengthen the time scale for the collapse. For the initial state of motion of the protogalaxy we have adopted the simplest assumption, i.e. pure uniform (solid body) rotation, the initial angular velocity being considered as a free parameter. We also assume that no external torques act on the system, so that its total angular momentum is conserved during the collapse.

As assumed in Papers I and II and further discussed by Larson (1975), we suppose that the gas in a protogalaxy is very clumpy and possesses large random or 'turbulent' motions. We have previously regarded the initial velocity dispersion of the random motions as a free parameter of the models, but in most of the present calculations the initial velocity dispersion has been set equal to the value given by the virial theorem. In partial justification of this assumption, we note that if the velocity dispersion were much smaller than this, it seems possible and perhaps even likely that gravitational forces acting within an irregular mass distribution would soon generate random velocities of the same order as the virial velocity. With the values assumed for the protogalactic mass and radius, the velocity dispersion in one coordinate direction given by the virial theorem is 55 km s^{-1}.

2.2 *Gaseous dissipation and star formation*

In Paper II, two prescriptions for the gaseous dissipation and star formation rates were found to yield models capable of reproducing the radial density structure of elliptical galaxies. In the approach used in Paper I and in Models F and I

of Paper II, the gaseous dissipation rate was calculated from a discrete cloud model for the gas motions and the star formation rate was assumed to vary as a power of the gas density, the best agreement with the observations being obtained with a value of about 1·8 for the exponent. Models calculated with these assumptions predict a metal abundance profile $Z(r)$ which decreases to very low values at large radii, and are perhaps in best agreement with the abundance gradient observed in the halo of our galaxy and that inferred for NGC 3379 from the observations of Burkhead & Kalinowski (1974). Models of this type also predict velocity distributions which are nearly isotropic at all radii, a result which may partially justify the assumption of an isotropic velocity distribution which has been adopted for simplicity in the present calculations (Section 3). For these reasons, most of the present calculations have adopted assumptions which are essentially the same as those of Model F of Paper II.

The other approach considered in Paper II, which has the advantage of being physically simpler and containing fewer parameters, was based on the assumption that the time scales for both gaseous dissipation and star formation are proportional to the local free-fall time. Models of this type generally predict smaller abundance gradients and higher metal abundances in the halos of galaxies, owing to the more efficient star formation occurring during the early stages of the collapse. Also, the velocity distribution is predicted to be significantly radially elongated at large radii. The properties of these models thus resemble to some extent those of the purely stellar models of Gott (1973, 1975) at large radii. Since it is not yet possible to rule out such models as applying to the halos of at least some galaxies, it is of interest to consider rotating models based on the same assumptions. Therefore we have calculated one model (Model 5) based on assumptions similar to those of Model B of Paper II.

2.3 '*Turbulent viscosity*'

If the protogalactic gas contains large random motions, as we have assumed, these random motions will transfer angular momentum from one part of the system to another and in general alter the distribution of angular momentum. We expect that angular momentum will usually be transported outward in a collapsing protogalaxy since, as was pointed out by McCrea (1960) in connection with his floccule theory of star formation, those gas elements which in a system of randomly moving elements happen to have little angular momentum will fall toward the centre and concentrate there, whereas the elements with large angular momentum will remain in the outer parts of the system. Thus there is a segregation of low and high angular momentum material, resulting in an outward transfer of angular momentum. As will be seen, it appears to be essential to assume significant outward transfer of angular momentum in a collapsing protogalaxy if realistic elliptical galaxy models are to be obtained.

In order to treat quantitatively the transfer of angular momentum in a collapsing protogalaxy, we have considered two possible descriptions of the gas motions, corresponding roughly to the limits of small and large mean free paths for the independently moving gas elements.

If the gas in a protogalaxy is distributed in many randomly moving discrete clouds, the system of clouds will possess a viscosity analogous to the molecular viscosity of a gas, except that the clouds here take the place of the molecules. In classical hydrodynamics, the motion of a viscous fluid is usually assumed to

be governed by the Navier–Stokes equations (e.g. Landau & Lifschitz 1959), which are derived on the assumption that the microscopic motions responsible for the viscosity have very small mean free paths, so that the viscous stress tensor depends only on the local shear of the velocity field. The Navier–Stokes equations imply that in an axisymmetric rotating system the viscous stress in the direction of rotation is proportional to the gradient of the angular velocity, and that angular momentum is transported outward in a system in which the angular velocity decreases outward.

The coefficient of kinematic viscosity ν appearing in the Navier–Stokes equations is given by the kinetic theory of gases as

$$\nu = \tfrac{1}{3}\bar{v}\lambda, \tag{1}$$

where $\bar{v}$ is the mean random velocity of the gas particles, and λ is the mean free path. To estimate the mean free path of the gas clouds in a protogalaxy, we consider the cloud model adopted in Paper I, which predicts that

$$\lambda = (8/\pi)^{1/2}\, C^{-1}\, \rho^{-1/2} \tag{2}$$

and

$$\nu = (8/3\pi)\, C^{-1}\, \rho^{-1/2}\, \alpha^{1/2} \tag{3}$$

where ρ is the average gas density, α is the mean squared random velocity in one coordinate direction, and C is a numerical coefficient estimated in Paper I to be about 3×10^{-3} in units such that the units of mass, length, and time are 1 $M_\odot$ 1 pc, and 10^6 yr respectively. The Navier–Stokes equations can be expected to provide a good approximation for the dynamics of the system if the mean free path given by equation (2) is small compared with the size of the system. Unfortunately this is not the case, as the value of λ predicted by equation (2) is typically of the order of 10^4 pc, and comparable with the length scale of the density distribution; thus the Navier–Stokes equations can at best provide only a crude order-of-magnitude approximation. Nevertheless, as will be seen, results calculated with the Navier–Stokes equations appear to be at least qualitatively correct when compared with the predictions of an alternative approach not based on the assumption of short mean free paths, and the models calculated in this way realistically resemble elliptical galaxies in structure. In the present calculations, the kinematic viscosity ν has been assumed to depend on ρ and α in the same way as predicted by equation (3):

$$\nu = C_\nu \rho^{-1/2}\, \alpha^{1/2} \tag{4}$$

where the coefficient C_ν is regarded as a free parameter, for which values between 100 and 250 have been tried (*cf.* the value of about 260 predicted by the cloud model of Paper I).

Because it is difficult to justify convincingly the applicability of the Navier–Stokes equations, we have considered also an alternative approach in which it is not assumed that the mean free paths of the gas clouds are small compared with the size of the system. The viscosity can then no longer be treated as a purely local effect related to the local shear of the velocity field, but we can still define the components of the viscous stress tensor in terms of the moments of the velocity distribution. These moments may be regarded as additional hydrodynamic variables whose space and time dependence are governed by moment equations derived from the Boltzmann equation. These moment equations are given and

discussed in the Appendix for the special case of a system with cylindrical symmetry. As is shown in the Appendix, these equations imply outward transport of angular momentum during at least the early stages of the collapse of a system of particles, even in the limit of long mean free paths.

Instead of solving these additional moment equations, we have attempted to find a simple analytic approximation for the relevant viscosity moment which predicts qualitatively the correct behaviour. One such expression is suggested if we assume that the clouds which fall toward the centre of the system possess atypically small angular momenta, while the clouds that carry most of the angular momentum remain in the outer regions. The rate of inward transport of angular momentum in the collapsing system is then considerably less than would be the case if there were no dispersion in the cloud angular momenta and all of the infalling clouds carried typical angular momenta; thus, associated with the random motions there is an outward transfer of angular momentum which is comparable with and partly cancels the inward transport of angular momentum by the mean flow. If w is the rotational velocity and u the radial velocity, the rate of transfer of angular momentum in the radial direction by the mean flow is proportional to $\langle u\rangle\langle w\rangle$, while the rate of transfer of angular momentum by random motions is proportional to $\delta_r = \langle(u-\langle u\rangle)(w-\langle w\rangle)\rangle$; the above argument then suggests that $\delta_r \propto -\langle u\rangle\langle v\rangle$. As discussed in the Appendix, this assumption predicts qualitatively the right dependence of δ_r on $\langle u\rangle$ and $\langle w\rangle$, so we have used expressions of this form to represent the components δ_r and δ_θ of the viscous stress, apart from geometrical factors and a constant of proportionality C_δ which has been treated as a free parameter (Appendix, equations A15).

2.4 *Gas recycling and metal enrichment*

Because the hydrodynamic calculations alone are already quite time consuming, the processes of stellar gas loss and heavy element production have been represented here by simple approximations rather than the more elaborate calculations used in Paper II. It was found in Paper II that gas loss from stars has little effect on the dynamics of the initial collapse or on the basic structure of the resulting galaxy; the main importance of gas recycling is in providing a continuing source of gas during the later stages of evolution of the system. Thus it is not very important to calculate the gas loss rate accurately during the first $\approx 10^9$ yr of evolution, but it may become more important during later stages. We have therefore sought a simple analytic formula which approximates the gas production rates calculated in Paper II at times $\gtrsim 10^9$ yr. The gas loss rates differ considerably between the different models of Paper II, but a representative approximation to these results is given by

$$\frac{d\rho_e}{dt} = 40\,\rho_s(t-500)^{-1.85} \qquad (5)$$

where $d\rho_e/dt$ is the gas loss rate per unit volume, ρ_s is the stellar mass density, and t is the time in units of 10^6 yr since the beginning of the collapse. This formula is generally accurate to within a factor of 2, and it is accurate to within 5 per cent for Model F at times $t \geqslant 3\times 10^9$ yr. The fraction of the total stellar mass which is returned to the interstellar medium within 10^{10} yr according to equation (5) is 0·22.

The rate of production of heavy elements has been calculated using the

'instantaneous recycling approximation', which assumes that the rate of production of heavy elements is proportional to the star formation rate; the 'yield', or ratio of the mass of heavy elements produced to the mass of stars formed, has been taken to be 0·02, which is approximately the value implied by the assumptions of Paper II. The contribution of non-instantaneous gas recycling to the chemical evolution has been neglected, and this leads to some inaccuracy in the calculation of the metal abundances during the later stages of evolution; however, it makes no important difference to the predicted composition gradients, which are our main interest here. The time and space dependence of the metal abundance of the gas have been calculated using equations similar to those of Paper II, generalized in an obvious way to the case of two space dimensions.

3. HYDRODYNAMICAL CALCULATIONS

As in Papers I and II, a collapsing protogalaxy is treated as a two-component system, and the gaseous and stellar components are described separately by hydrodynamic equations derived from the Boltzmann equation. We assume axial symmetry and adopt spherical polar coordinates r, θ, ϕ, with corresponding velocity components $u = \dot{r}$, $v = r\dot{\theta}$, $w = r \sin\theta\dot{\phi}$; this coordinate system seems best suited for describing a system that is expected to become highly centrally condensed. In order to keep the number of variables and equations to a minimum, we have made the important simplifying assumption that the velocity distributions of both gas and stars are isotropic; this is approximately the case in the models of Paper I and in Models F and I of Paper II. There are then five variables to be calculated as functions of space and time for both gas and stars: the mean density ρ, the three components $\langle u\rangle$, $\langle v\rangle$, and $\langle w\rangle$ of the mean velocity, and the mean squared random velocity α in one coordinate direction. In addition, the gravitational potential Φ must be calculated by solving the Poisson equation simultaneously with the hydrodynamic equations.

For an axisymmetric system, the Eulerian equations of fluid dynamics in spherical coordinates can be written, for either gas or stars,

$$\frac{\partial\rho}{\partial t}+\frac{1}{r^2}\frac{\partial}{\partial r}r^2\rho\langle u\rangle+\frac{1}{r\sin\theta}\frac{\partial}{\partial\theta}\sin\theta\,\rho\langle v\rangle=\mathscr{S}(\rho) \tag{6}$$

$$\frac{\partial\langle u\rangle}{\partial t}+\langle u\rangle\frac{\partial\langle u\rangle}{\partial r}+\frac{\langle v\rangle}{r}\frac{\partial\langle u\rangle}{\partial\theta}+\frac{1}{\rho}\frac{\partial}{\partial r}\rho\alpha+\frac{\partial\Phi}{\partial r}-\frac{\langle v\rangle^2+\langle w\rangle^2}{r}=\mathscr{S}(u) \tag{7}$$

$$\frac{\partial\langle v\rangle}{\partial t}+\frac{\langle u\rangle}{r}\frac{\partial}{\partial r}r\langle v\rangle+\frac{\langle v\rangle}{r}\frac{\partial\langle v\rangle}{\partial\theta}+\frac{1}{\rho r}\frac{\partial}{\partial\theta}\rho\alpha+\frac{1}{r}\frac{\partial\Phi}{\partial\theta}-\frac{\langle w\rangle^2}{r\tan\theta}=\mathscr{S}(v) \tag{8}$$

$$\frac{\partial\langle w\rangle}{\partial t}+\frac{\langle u\rangle}{r}\frac{\partial}{\partial r}r\langle w\rangle+\frac{\langle v\rangle}{r\sin\theta}\frac{\partial}{\partial\theta}\sin\theta\langle w\rangle+\frac{1}{r^3\rho}\frac{\partial}{\partial r}r^3\rho\delta_r$$
$$+\frac{1}{\rho r\sin^2\theta}\frac{\partial}{\partial\theta}\sin^2\theta\rho\delta_\theta=\mathscr{S}(w) \tag{9}$$

$$\frac{\partial\alpha}{\partial t}+\langle u\rangle\frac{\partial\alpha}{\partial r}+\frac{\langle v\rangle}{r}\frac{\partial\alpha}{\partial\theta}+\frac{2}{3}\frac{\alpha}{r^2}\frac{\partial}{\partial r}r^2\langle u\rangle+\frac{2}{3}\frac{\alpha}{r\sin\theta}\frac{\partial}{\partial\theta}\sin\theta\langle v\rangle=\mathscr{S}(\alpha). \tag{10}$$

The quantities $\mathscr{S}(\rho)$, $\mathscr{S}(u)$, etc. on the right-hand sides of equations (6)–(10) are source terms representing the effects on ρ, $\langle u\rangle$, etc., of gaseous dissipation, star

formation, and stellar mass loss; these terms are different for the gas and for the stars, and are given below. The quantities $\rho\delta_r$ and $\rho\delta_\theta$ in equation (9) are the components of the viscous stress tensor in the direction of rotation, and are defined by

$$\left.\begin{aligned}\delta_r &= \langle(u-\langle u\rangle)(w-\langle w\rangle)\rangle \\ \delta_\theta &= \langle(v-\langle v\rangle)(w-\langle w\rangle)\rangle.\end{aligned}\right\} \tag{11}$$

Expressions for δ_r and δ_θ in the two approximations considered are given in the Appendix (equations (A14) and (A15)). Terms expressing the effect of viscosity on $\langle u\rangle$, $\langle v\rangle$, and α have been omitted from the above equations because they appear to play a less essential role in the dynamics. In addition to the above hydrodynamic equations, we also have the Poisson equation for the gravitational potential Φ:

$$\nabla^2\Phi = \frac{1}{r^2}\frac{\partial}{\partial r}\left(r^2\frac{\partial\Phi}{\partial r}\right)+\frac{1}{r\sin\theta}\frac{\partial}{\partial\theta}\left(\sin\theta\,\frac{1}{r}\frac{\partial\Phi}{\partial\theta}\right) = 4\pi G\rho_t \tag{12}$$

where ρ_t is the total density of both gas and stars.

The source terms $\mathscr{S}(\rho)$, $\mathscr{S}(u)$, etc. for the gas are given as in Paper II by the following expressions, where $d\rho_s/dt$ denotes the star formation rate, $d\rho_e/dt$ the stellar gas loss rate, $d\alpha_g/dt$ the gaseous dissipation rate, and the subscripts g and s refer to the gas and the stars respectively:

$$\mathscr{S}(\rho_g) = -\frac{d\rho_s}{dt}+\frac{d\rho_e}{dt} \tag{13}$$

$$\mathscr{S}(u_g) = \frac{1}{2\rho_g}(\langle u_s\rangle-\langle u_g\rangle)\frac{d\rho_e}{dt} \tag{14}$$

with similar expressions for $\mathscr{S}(v_g)$ and $\mathscr{S}(w_g)$, and

$$\mathscr{S}(\alpha_g) = \frac{d\alpha_g}{dt}+\frac{1}{\rho_g}(\alpha_s-\alpha_g)\frac{d\rho_e}{dt}. \tag{15}$$

For the stars we have

$$\mathscr{S}(\rho_s) = \frac{d\rho_s}{dt}-\frac{d\rho_e}{dt} \tag{16}$$

$$\mathscr{S}(u_s) = \frac{1}{\rho_s}(\langle u_g\rangle-\langle u_s\rangle)\frac{d\rho_s}{dt}, \text{ etc.} \tag{17}$$

$$\mathscr{S}(\alpha_s) = \frac{1}{\rho_s}\left\{(\alpha_g-\alpha_s)+\frac{1}{3}[(\langle u_g\rangle-\langle u_s\rangle)^2+(\langle v_g\rangle-\langle v_s\rangle)^2+(\langle w_g\rangle-\langle w_s\rangle)^2]\right\}\frac{d\rho_s}{dt}. \tag{18}$$

In these expressions, the star formation rate $d\rho_s/dt$ and the gaseous dissipation rate $d\alpha_g/dt$ have been calculated according to the assumptions described in Section 2.2, and the stellar gas loss rate $d\rho_e/dt$ is given by equation (5).

The method that has been used for solving the hydrodynamic equations is an adaptation of that developed by Larson (1972b) for calculating the collapse of a rotating gas cloud. A fixed Eulerian grid is defined, with 20 divisions in the r-direction spaced at equal intervals of 0·15 in log r, and 10 divisions in the θ-direction between $\theta = 0$ and $\theta = \pi/2$, spaced slightly more closely near the

equatorial plane $\theta = \pi/2$. The hydrodynamic partial differential equations are approximated by implicit difference equations, using backward time differences to avoid an unduly restrictive Courant condition on the time step. The difference equations are, as far as possible, a direct generalization of the much simpler one-dimensional difference equations given in Paper I. The implicit hydrodynamic equations and the Poisson equation are solved simultaneously during each time step by the standard Newton–Raphson linearization technique, and the resulting large set of linear equations is solved by an alternating-direction iterative method. As in Paper I, in calculating each time step the variables describing the gas and the gravitational potential Φ are first advanced, assuming no change in the stellar distribution; then the gas distribution is left unchanged while the variables describing the stars are advanced and Φ is recalculated. After all of the hydrodynamic variables have been advanced, the metal abundances Z_g and Z_s of the gas and stars are advanced by a relatively simple separate calculation as in Paper II.

4. RESULTS AND COMPARISON WITH OBSERVATIONS

4.1 *Model without viscosity*

To illustrate the importance of including the viscosity effect discussed in Section 2.3, we present first the results of a calculation in which viscosity is neglected. The initial conditions assumed for this model are those described in Section 2.1, with an initial angular velocity of $\omega_0 = 0{\cdot}002\ (10^6\ \mathrm{yr})^{-1}$; this gives the protogalaxy an initial equatorial rotational velocity of 60 km s^{-1} and an angular momentum per unit mass somewhat less than that of the disc of our galaxy. The gaseous dissipation rate is given by the cloud model of Paper I, and the star formation law is that of Models F and I of Paper II, except for a slightly smaller numerical coefficient:

$$\frac{d\rho_s}{dt} = 0{\cdot}55\ \rho_g^{1{\cdot}85}. \tag{19}$$

The early stages of collapse of this inviscid model are qualitatively similar to the non-rotating case, since centrifugal force is initially too weak to balance gravity; the system thus begins to collapse almost radially and become centrally condensed. The first generations of stars thus form in an extended, nearly spherical, slowly rotating halo. As the remaining gas continues to fall inward, its rotational velocity increases and it acquires a more and more flattened distribution, finally forming a thin flat disc in the innermost several kiloparsecs of the system. Thus successive generations of stars are formed with more and more flattened spatial distributions, ending with the formation of a remarkably flat, uniform stellar disc in the inner part of the system. The contours of equal stellar density in one quadrant of a meridional plane are shown in Fig. 1 for a time about $1{\cdot}6 \times 10^9$ yr ($\sim$6 free-fall times) after the beginning of the collapse, when all but 3 per cent of the total mass has been converted into stars. This result is typical of several models calculated without viscosity but with various choices of the other model assumptions.

It is immediately evident that the resulting model does not at all resemble an elliptical galaxy: the central part of the system is much too flat, and there is no condensed nucleus. While the occurrence of non-axisymmetric instabilities

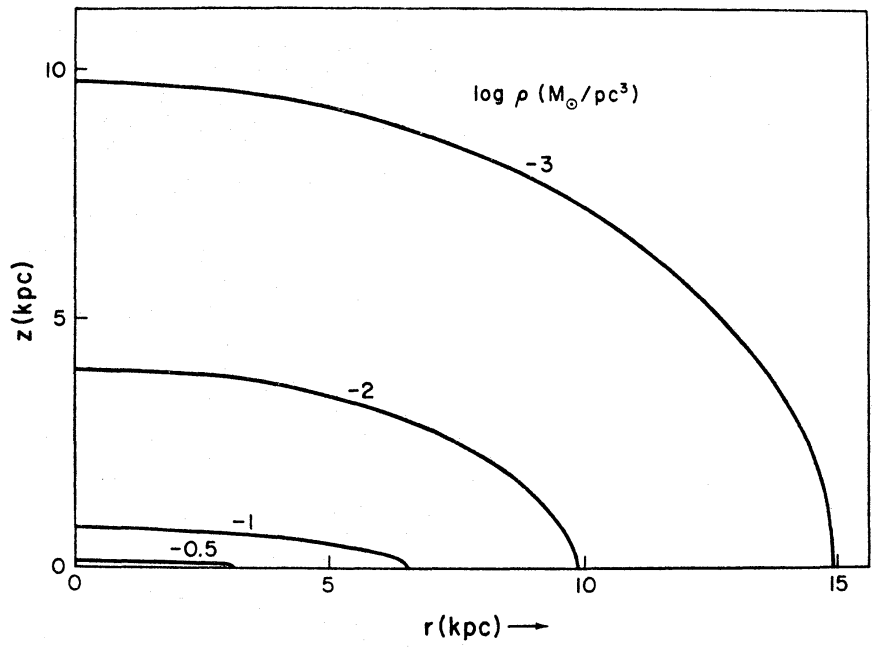

FIG. 1. *Contours of equal stellar density ρ in one quadrant of a meridional plane for a model calculated without viscosity. The curves are labelled with the logarithm of the stellar density in units of* $M_\odot\, pc^{-3}$.

in such a highly-flattened configuration would almost certainly lead to the outward transport of angular momentum by gravitational torques, and hence to the formation of a more centrally-condensed disc possibly resembling those seen in spiral galaxies (Hohl 1971), such a model could still not explain the formation of *elliptical* galaxies with only moderate flattening throughout, unless the disc is somehow thickened into a spheroidal configuration at the same time. In any case it seems clear that a model which allows no internal redistribution of angular momentum cannot explain the formation of elliptical galaxies with the observed properties; some form of outward transport of angular momentum is required, whether by viscosity or by gravitational torques or both. Since the models never become very flattened when a realistic viscosity is included (see below), and since it is difficult to estimate the possible effect of gravitational torques, we shall assume for purposes of calculation that the dominant mechanism of angular momentum transfer is the 'turbulent viscosity' effect discussed above (Section 2.3).

4.2 *Model with viscosity*

We now describe the results obtained for Model 1, a typical model incorporating a finite viscosity but otherwise identical in its assumptions to the inviscid model described above. The viscosity effect has been treated using the Navier–Stokes equations with a kinematic viscosity given by equation (4) with $C_\nu = 150$, a somewhat smaller viscosity than predicted by the cloud model of Paper I ($C_\nu \sim 260$). The stellar density distribution obtained for Model 1 is shown in Fig. 2(a) for a time about 3×10^9 yr (~ 11 free-fall times) after the beginning of the collapse, when only about 2 per cent of the total mass remains in the form of gas. The predicted amount and distribution of residual gas at this time are probably not very reaslistic, since the viscosity given by equation (4) becomes unrealistically large when the gas density becomes low; in any case it is likely that an elliptical

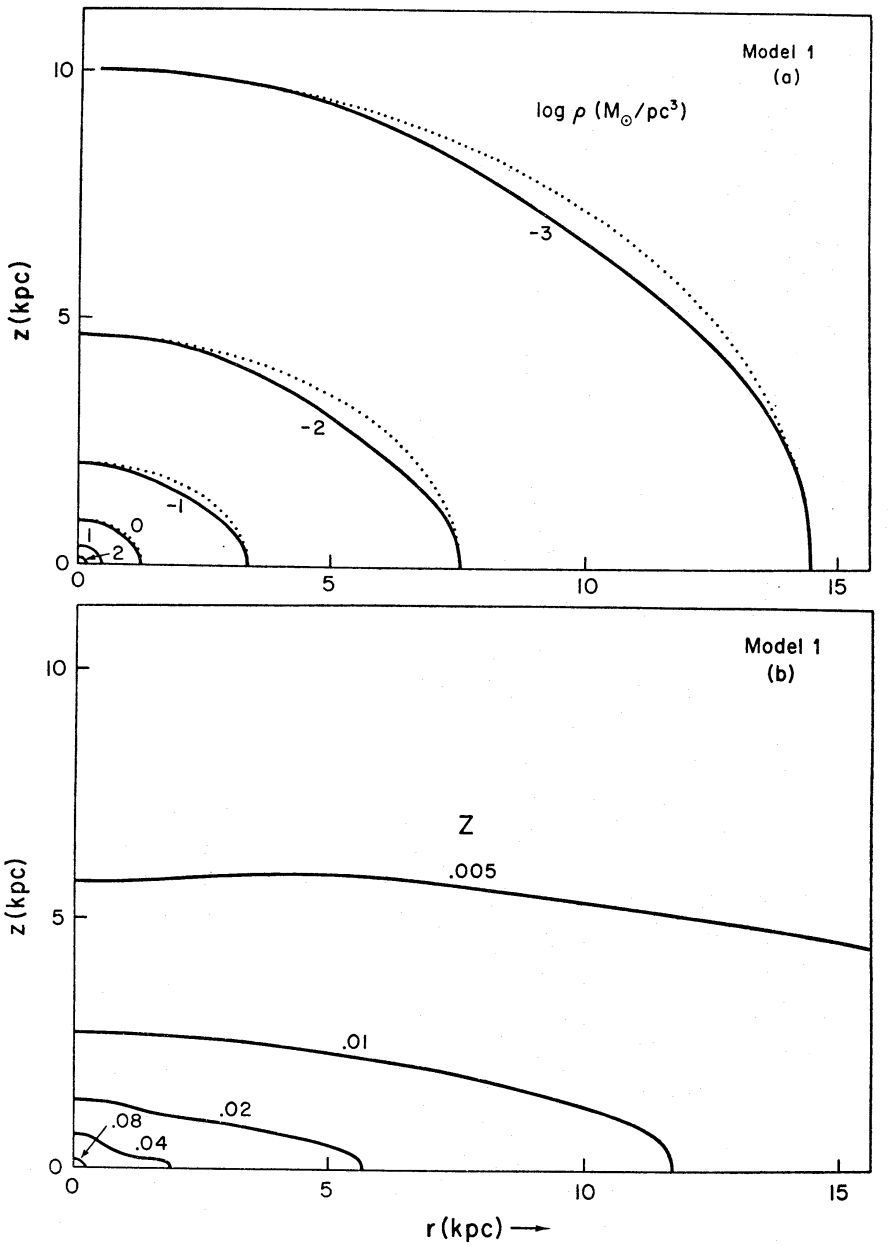

FIG. 2. (*a*) *Contours of equal stellar density* ρ *in a meridional plane for a typical model with viscosity, Model* 1 (*solid curves*). *The dotted curves are ellipses with the same major and minor axes.* (*b*) *Contours of average stellar metal abundance Z in a meridional plane for Model* 1.

galaxy will have lost its gas by this time (Larson 1974b; Gisler 1975), so we shall neglect this residual gas and consider only the properties of the stellar system formed by this time.

It is evident in Fig. 2(a) that the density distribution of Model 1 now closely resembles that of an elliptical galaxy. Instead of increasing to very high values, the ellipticity $\epsilon(=1-b/a)$ of the density contours now actually decreases toward the centre, and the system has a highly condensed and nearly round nucleus resembling those typically observed in E galaxies. From the ellipticity profile $\epsilon(r)$ of Model 1, illustrated in Fig. 5(a), we see that ϵ is less than 0·1 near the centre, increases to a maximum of about 0·4 at $r \sim 5$ kpc, and then decreases

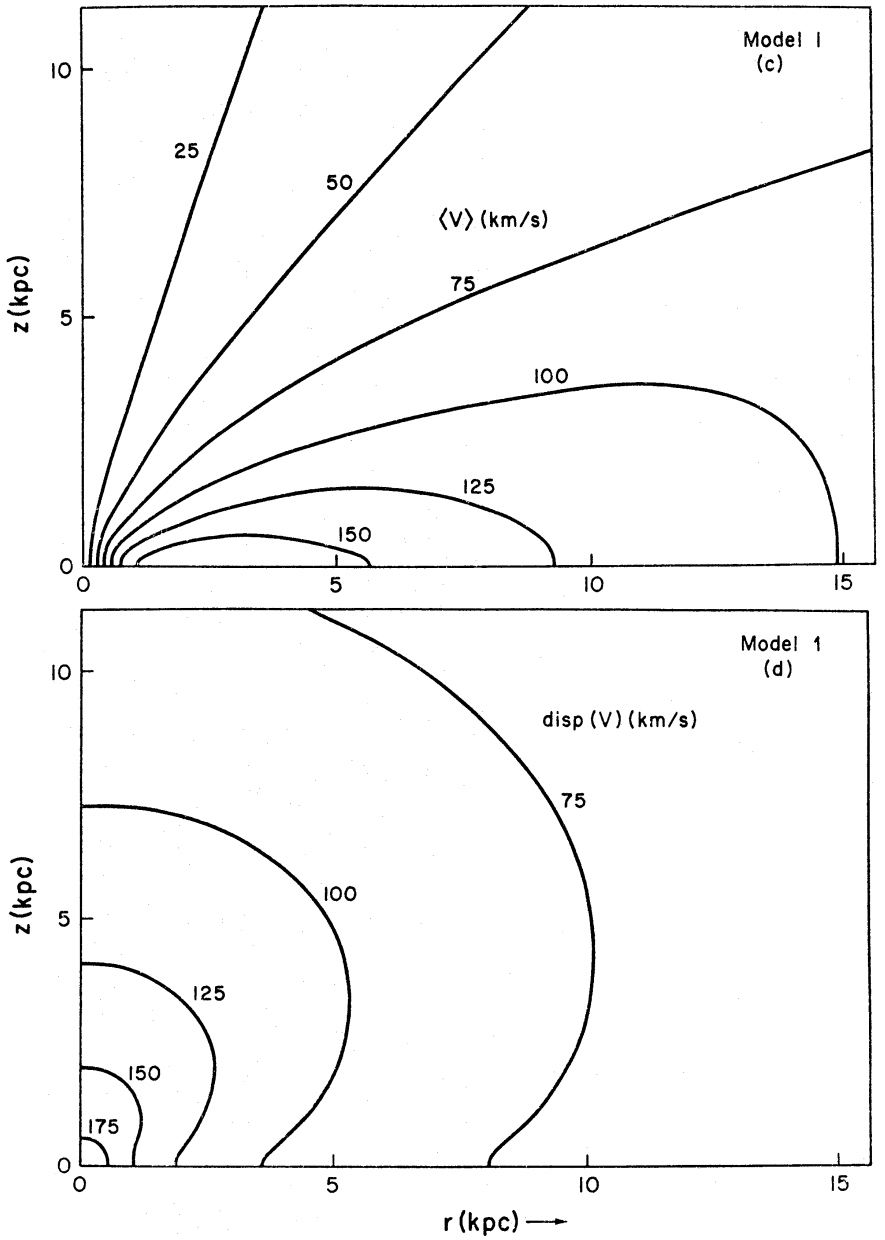

FIG. 2. (*c*) *Contours of average stellar rotational velocity* $\langle V \rangle$ *in a meridional plane for Model* 1, *in units of km* s^{-1}. (*d*) *Contours of stellar velocity dispersion disp* $(V) = \alpha^{1/2}$ *(assumed isotropic) in a meridional plane for Model* 1, *in units of km* s^{-1}.

slightly to about 0·3 at the outer boundary. Although different elliptical galaxies differ considerably in their ellipticity profiles (see below), this qualitative behaviour is observed in a number of E galaxies, and has been considered by some authors to be characteristic of E galaxies in general (e.g. de Vaucouleurs 1959; Liller 1960).

The density contours shown in Fig. 2(a) deviate slightly but significantly from perfect ellipses (dotted curves) in that they are slightly more pointed toward the ends of the major axis and have slightly smaller areas than ellipses with the same axes. This effect is seen also in the contours of projected surface density, which are not shown separately because they are very similar in appearance to the density contours shown in Fig. 2(a). This prediction agrees qualitatively with

the observed isophotal shapes of E and So galaxies, which characteristically deviate in the same way from perfect ellipses (e.g. de Vaucouleurs 1959; van Houten 1961; Liller 1966).

The radial structure of Model 1 is very similar to that of the spherical models of Paper II. The radial profiles of projected surface density $\sigma(r)$ for both equatorial and polar projections are given by the uppermost set of curves in Fig. 7. Although the model parameters have not been adjusted to optimize the fit to observed surface brightness profiles, and although the central density is not quite as high as in the models of Paper II, the general resemblance to the observations is nevertheless still quite close, particularly for the polar projection (dashed curve) which matches closely the mean profile of 14 elliptical galaxies as determined by King (1975, in preparation). The fact that the present rotating models predict nearly the same radial structure as the previous spherical models supports the assumption of Papers I and II that the radial structure of elliptical galaxies can be adequately approximated with spherical non-rotating models.

Fig. 2(b), (c) and (d) illustrate the distributions of average stellar metal abundance Z, average rotational velocity $\langle V \rangle$, and velocity dispersion

$$\text{disp}\,(V) = \alpha^{1/2}$$

in a meridional plane of Model 1. The corresponding projected distributions have also been calculated but are not shown separately because they resemble closely the distributions plotted in Fig. 2(b)–(d). In Fig. 2(b) we see that, as in the spherical models, the average stellar metal abundance Z decreases with distance from the centre, but the metal abundance distribution is also strongly flattened toward the equatorial plane, much more so than the density distribution. This strong flattening of the metal abundance distribution arises because during the later stages of the collapse the inflow of gas takes place predominantly in a direction perpendicular to the equatorial plane, concentrating the heavy elements toward this plane and establishing a composition gradient which is primarily in the perpendicular direction. Near the centre, the inflow of gas is more nearly radial, so the composition gradient is also more nearly radial. The prediction that rotating galaxies should possess flattened metal abundance distributions is in qualitative agreement with the observation by Spinrad, Smith & Taylor (1972) that the CN band strength in the So galaxy NGC 3115 has a steeper gradient along the minor axis than along the major axis.

In Fig. 2(c) we see that the contours of average rotational velocity $\langle V \rangle$ are also flattened toward the equatorial plane. Large rotational velocities and strong differential rotation are present in the equatorial plane, but $\langle V \rangle$ decreases rapidly away from this plane, and the halo part of the system rotates much more slowly and more nearly uniformly. Fig. 2(d) shows that, superimposed on a general trend of decreasing velocity dispersion with increasing distance from the centre, there is an increase in velocity dispersion with distance from the equatorial plane, so that at a given distance from the centre the velocity dispersion is smallest in the equatorial plane. The relatively high rotational velocity and small velocity dispersion in the equatorial plane of this model are responsible for the slightly pointed appearance of the density contours shown in Fig. 2(a).

All of the model characteristics outlined above can be roughly but conveniently summarized by describing the system as being made up of a sequence of stellar populations ranging from a nearly spherical, slowly rotating, metal poor ' halo

population' to a much more flattened, rapidly rotating, and metal rich 'disc population' with a relatively small velocity dispersion. This population sequence directly reflects the evolution of the protogalactic gas distribution from an extended, nearly spherical cloud to a rapidly rotating flat layer in the equatorial plane, with the concurrent enrichment of this gas in heavy elements.

4.3 *Effect of model parameters*

In this section we present results for a number of models based on the same assumptions as Model 1 except for different values of the initial angular velocity ω_0 and the viscosity parameter C_ν. The stellar density distributions for two of these models are illustrated in Figs 3 and 4. Model 2 (Fig. 3) is calculated with

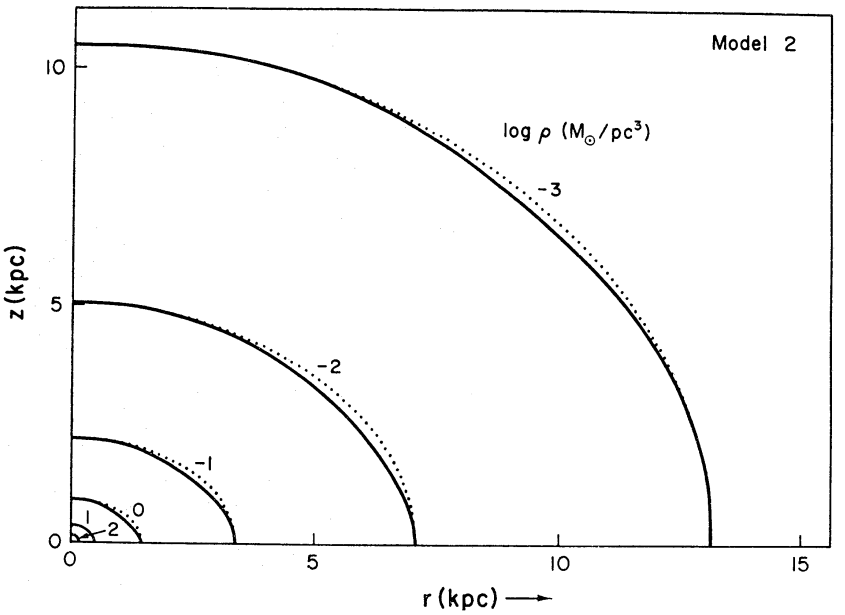

FIG. 3. *Contours of equal stellar density for Model 2. Dotted curves are ellipses with the same axes.*

an initial angular velocity $\omega_0 = 0{\cdot}001\,33\ (10^6\ \mathrm{yr})^{-1}$ which is 2/3 as large as for Model 1, and a viscosity parameter $C_\nu = 100$ which is also somewhat smaller. As expected, the ellipticity of Model 2 is considerably smaller than that of Model 1 at most radii, except near the centre where it is slightly larger. Model 3 (Fig. 4), with $\omega_0 = 0{\cdot}003\ (10^6\ \mathrm{yr})^{-1}$ and $C_\nu = 100$, is the most rapidly rotating and flattest model calculated; its maximum ellipticity is about 0·6 at $r \sim 5$ kpc, so it corresponds to an E6 galaxy, which is about the flattest form observed for true elliptical galaxies.

Comparing the density distributions shown in Figs 2(a), 3 and 4 for models with different initial angular velocities and different ellipticities, we see that the density contours deviate more and more from perfect ellipses as the ellipticity increases. This reflects the increasing importance of a relatively flattened, disc-like component in the models, and is in qualitative agreement with the observed trend in the isophotal shapes of E and So galaxies. A quantitative measure of the deviation of galaxy isophotes from ellipses has been defined by Liller (1966), who gives the ratio of the area of each isophote to the area of an ellipse with the same axes;

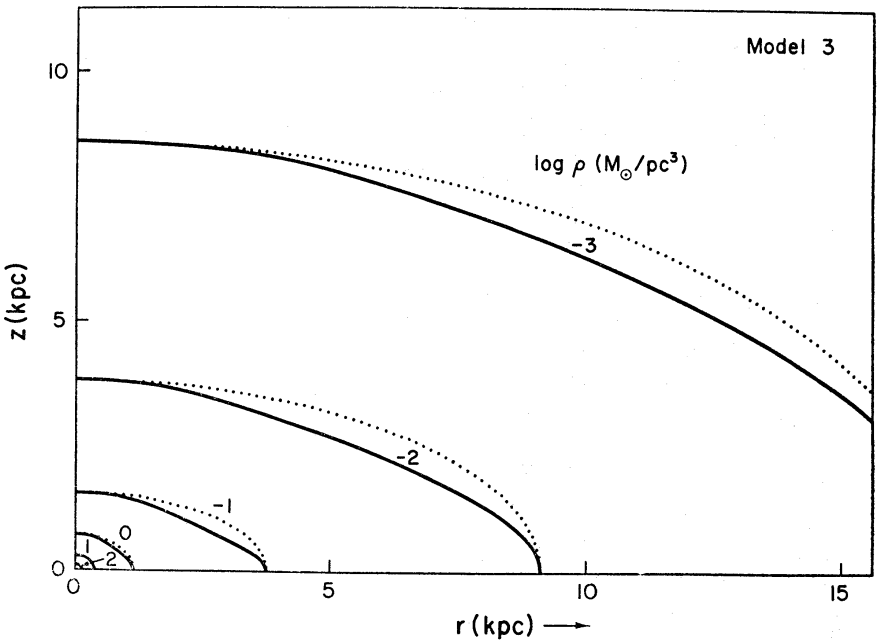

FIG. 4. *Contours of equal stellar density for Model 3. Dotted curves are ellipses with the same axes.*

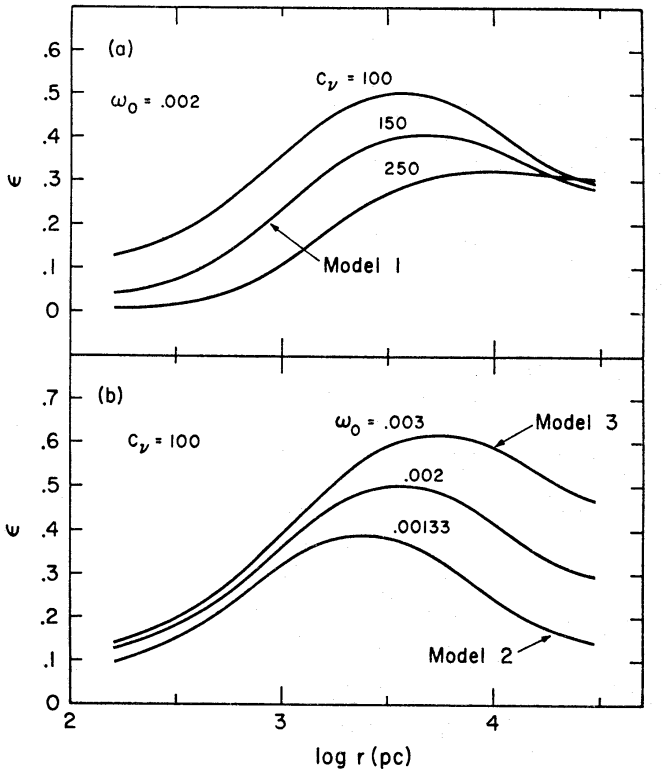

FIG. 5. *Model ellipticity profiles: the ellipticities* $\epsilon = 1 - b/a$ *of the density contours plotted* vs *their semi-major axes r. (a) Ellipticity profiles* $\epsilon(r)$ *for 3 models with the same initial angular velocity* $\omega_0 = 0{\cdot}002\ (10^6\ yr)^{-1}$, *but with different values of the viscosity parameter* C_ν *as indicated. (b) Ellipticity profiles for 3 models with the same viscosity parameter* C_ν *but different values of the initial angular velocity* ω_0.

according to these data, the ratio of areas is usually close to 1·00 for ellipticities less than about 0·3, but it may have values ranging down to about 0·80 for ellipticities of 0·6 or greater. For comparison, the ratio of areas in the models ranges from 0·99 for the log $\rho = -3$ contour of Model 2 ($\epsilon = 0{\cdot}20$) to 0·85 for the log $\rho = -1$ contour of Model 3 ($\epsilon = 0{\cdot}58$). Thus the predicted variation of the ratio of areas appears to be at least roughly consistent with the observations.

Fig. 5 shows the ellipticity profiles $\epsilon(r)$ obtained for several models calculated with various values of the viscosity parameter C_ν and the initial angular velocity ω_0, including Models 1, 2, and 3. Fig. 5(a) shows the effect of increasing the viscosity parameter C_ν: this hardly alters the ellipticity near the outer boundary, but substantially decreases the ellipticity at smaller radii. A family of ellipticity profiles is generated, ranging from a strongly-peaked profile if $C_\nu < 100$, through a profile which becomes nearly flat at large radii if $C_\nu \sim 250$, to a profile which increases monotonically with radius if $C_\nu > 250$. Fig. 5(b) shows the effect of increasing the initial angular velocity ω_0 : this increases the ellipticity of the outer part of the system, but has relatively little effect on $\epsilon(r)$ near the centre. Thus, at least for this class of models, the ellipticity of the outer part of the system depends mainly on the initial angular velocity, whereas the ellipticity of the inner regions depends mainly on the amount of viscous redistribution of angular momentum that takes place during the collapse. By varying the parameters ω_0 and C_ν it is possible to generate a considerable variety of ellipticity profiles, but there remains a general tendency for models of this type to predict ellipticities which are small near the centre and peaked at intermediate radii.

It is difficult to make any quantitative comparison between predicted and observed ellipticity profiles because the observed ellipticity profiles of E galaxies are quite diverse in form (Liller 1960, 1966; Rood & Baum 1968; Wilson 1975; King 1975, in preparation). Nearly every kind of ellipticity profile is found: peaked, nearly flat, monotonically increasing, monotonically decreasing, and more complicated forms. More often than not, however, the ellipticity is smallest near the centre and increases outward; at larger radii, $\epsilon(r)$ may either pass through a maximum, become nearly constant, or continue to increase monotonically. The most highly-flattened systems generally tend to have peaked $\epsilon(r)$ profiles. These regularities in the data are qualitatively consistent with the model predictions illustrated in Fig. 5.

The rotation curves of these models are illustrated in Fig. 6. In Fig. 6(a), which shows results for the same models as Fig. 5(a), we see that the models with larger C_ν, which have smaller ellipticities at most radii, also have lower rotational velocities at most radii. However, the differences between the rotation curves are not large: in all cases the maximum rotational velocity lies between 150 and 178 km s^{-1} and occurs at a radius between 2·2 and 2·5 kpc, and is followed by a gradual decline in rotational velocity at larger radii. Fig. 6(b) shows that when the initial angular velocity ω_0 is increased, the rotational velocity in the outer part of the system increases, but the maximum rotational velocity nearer the centre actually decreases. This decrease in the peak velocity occurs because in the models with larger ω_0 the mass is somewhat more widely distributed, and there is less mass in the innermost few kiloparsecs of the system.

Unfortunately there are very few observations with which such predicted rotation curves may be compared, and some of the data have significant uncertainties. For a few E galaxies the central slope of the rotation curve has been measured

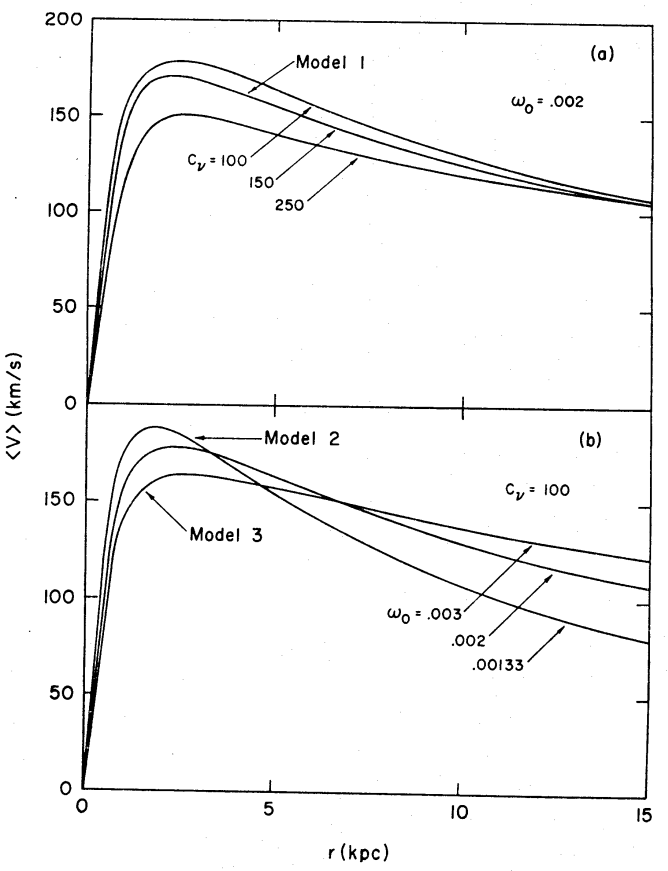

FIG. 6. (*a*) *Curves of average stellar rotational velocity* $\langle V \rangle$ vs r *in the equatorial plane of* 3 *models with the same* ω_0 *but varying* C_ν, *as in Fig.* 5(*a*). (*b*) *Rotation curves in the equatorial plane for* 3 *models with the same* C_ν *but varying* ω_0, *as in Fig.* 5(*b*).

(King & Minkowski 1966; Morton & Chevalier 1973), and values ranging from about 150 to 400 km s^{-1} kpc^{-1} are found; for comparison, the central slopes of the rotation curves shown in Fig. 6 vary from 130 to 240 km s^{-1} kpc^{-1}. If the model parameters had been adjusted to give slightly higher and more realistic central densities, larger central slopes would have been predicted. The only available rotation curve for an elliptical galaxy has been obtained by Bertola & Capaccioli (1975) for the E5 galaxy NGC 4697, but the maximum rotational velocity determined by these authors is only 65 km s^{-1}; as was found by Gott (1975), it is difficult to reconcile this low rotational velocity with the high ellipticity for any reasonable dynamical model, unless the measured velocity dispersion of 310 km s^{-1} is too large. Clearly, more data for velocity dispersions and rotational velocities in elliptical galaxies will be required before it is possible to make much of comparisons between predicted and observed rotation curves.

The profiles of projected surface density $\sigma(r)$ for Models 1, 2 and 3 are shown in Fig. 7 for both equatorial and polar projections. For comparison, the dotted straight line is the power law $\sigma \propto r^{-1.65}$, which approximately matches the spherical models of Paper II and the E1 galaxy NGC 3379 over a considerable range of radii. Although the model parameters have not been adjusted to optimize the agreement with observations, the agreement is still qualitatively satisfactory, particularly for Model 1. The agreement with observations is also generally better for the predicted $\sigma(r)$ profile along the minor axis (lower solid curve) or

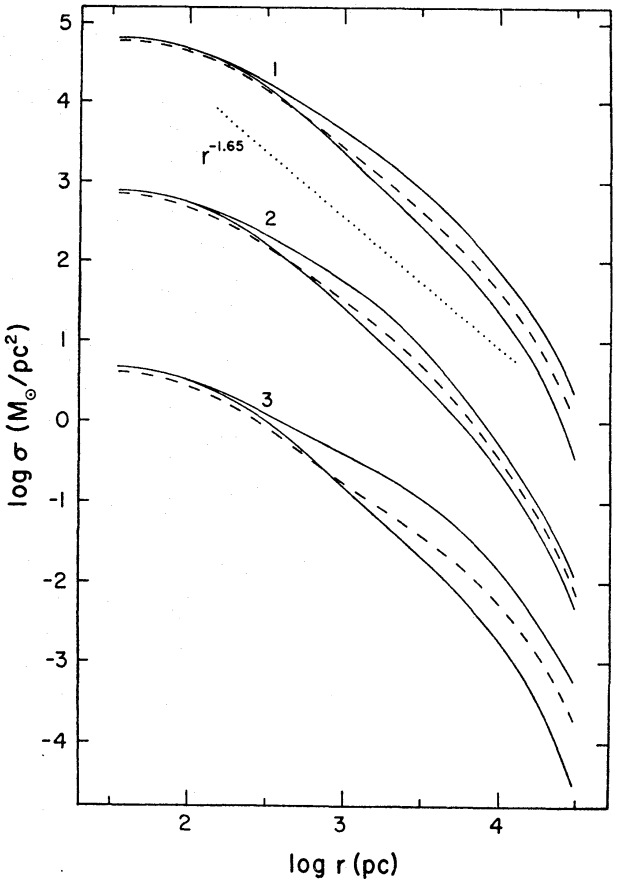

FIG. 7. *Profiles of projected stellar surface density* $\sigma(r)$ *for Models* 1, 2 *and* 3. *In each set of curves the two solid curves give the profiles predicted for the major axis (upper curve) and minor axis (lower curve) in an equator-on view, and the dashed curve gives the profile predicted for a pole-on view. The scale at left is for the top set of curves (Model* 1*); the curves for Models* 2 *and* 3 *are displaced successively downward by* 2 *units in log* σ.

for the polar projection (dashed curve) than for the major axis profile (upper solid curve), which shows greater curvature in a logarithmic plot. This is particularly true for the flattest model, Model 3, whose major axis profile is intermediate between a power law and an exponential law. The curvature of the major axis profile reflects the varying contribution of a flattened component in the models: the flattened component is unimportant near the centre, reaches its maximum prominence at radii of several kpc where the ellipticity is a maximum, and then becomes less important again at larger radii.

4.4 *Effect of the treatment of viscosity*

In this section we present results for Model 4, which is based on the same assumptions as Model 1 except for the treatment of viscosity, which follows the alternative way of approximating the moments of the velocity distribution discussed in Section 2.3 and the Appendix. The moments δ_r and δ_θ giving the components of viscous stress in the direction of rotation are assumed to be given by equations (A15), and the dimensionless parameter C_δ has been set equal to 0·4. During the later stages of the collapse this approximation should be more realistic than the Navier–Stokes equations with a kinematic viscosity given by

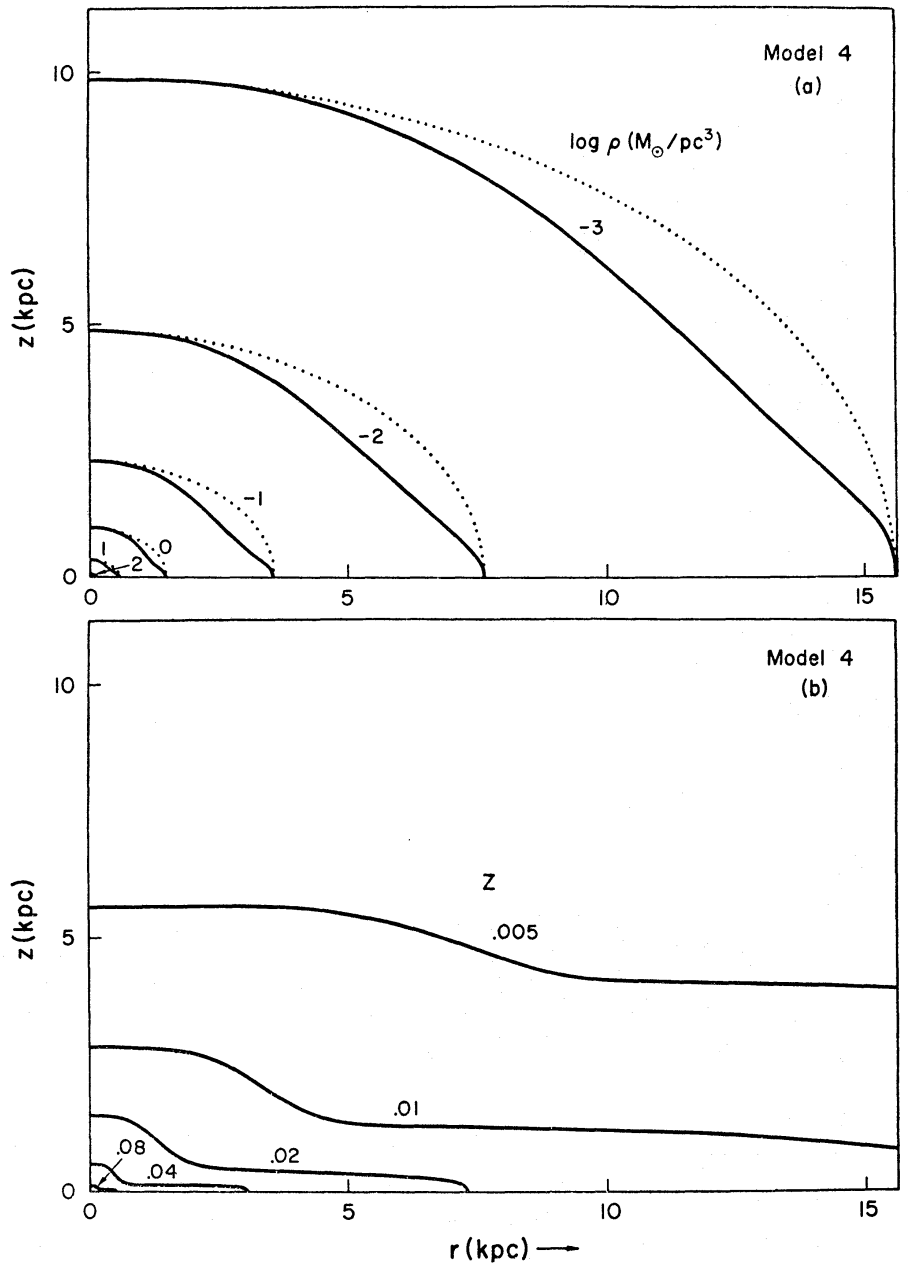

FIG. 8. (*a*) *Contours of equal stellar density in a meridional plane for Model* 4. *Dotted curves are ellipses with the same axes.* (*b*) *Contours of average stellar metal abundance Z for Model* 4.

equation (4), since equation (4) implies that the viscosity increases to unrealistically high values as the gas density decreases; on the other hand, equations (A13) or (A15) predict that the viscosity becomes small as the gas settles into an equilibrium disc, in which one might expect ' turbulent viscosity ' to become less important.

The distributions of stellar density, metal abundance, rotational velocity, and velocity dispersion in Model 4 are illustrated in Fig. 8(a)–(d), which may be compared with the results for Model 1 shown in Fig. 2(a)–(d). We see that Model 4 shows more prominently than Model 1 the presence of a highly-flattened disc-like component with high metal abundance, high rotational velocity, and low velocity dispersion. This is because during the later stages of the evolution of Model 4

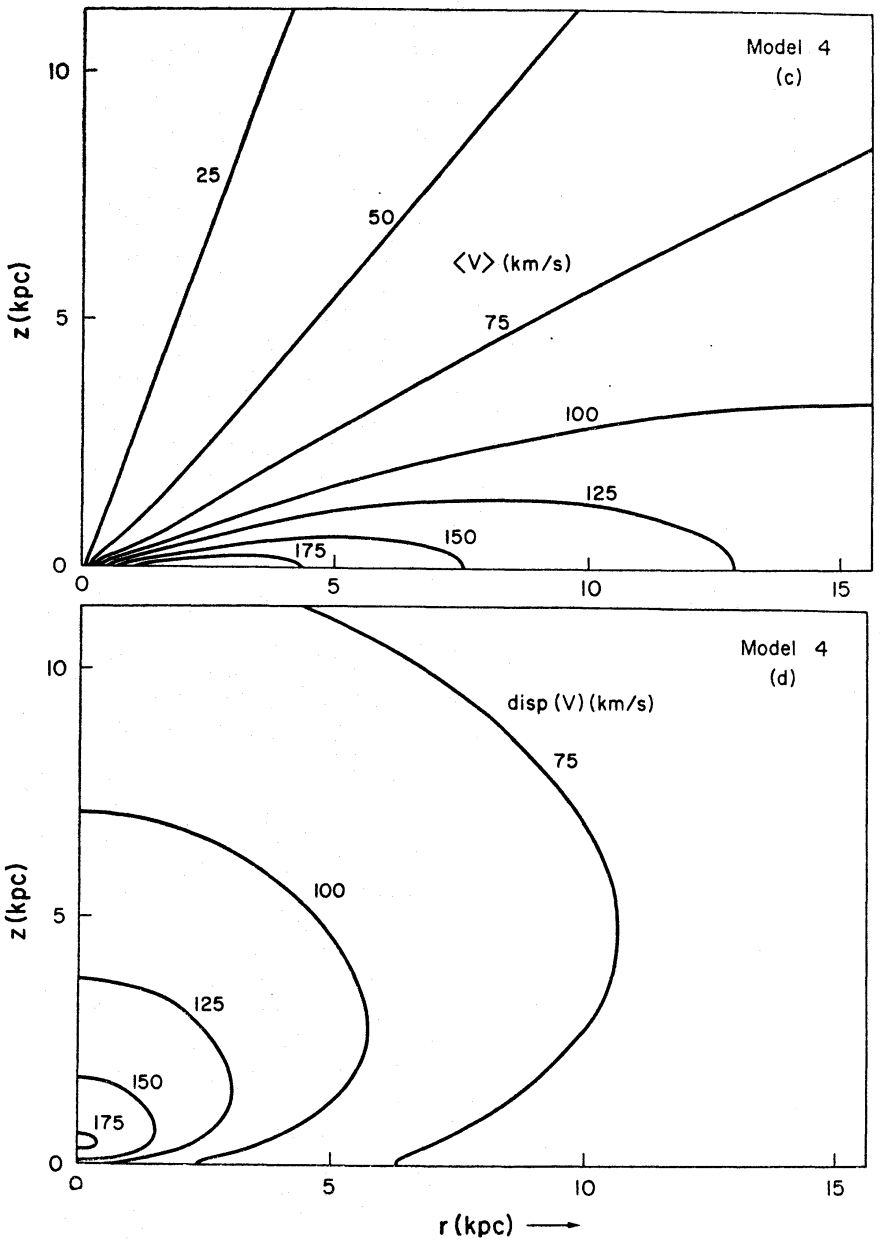

FIG. 8. (*c*) *Contours of average stellar rotational velocity* $\langle V \rangle$ *for Model* 4. (*d*) *Contours of stellar velocity dispersion disp* $(V) = \alpha^{1/2}$ *for Model* 4.

most of the residual gas settles into and remains in a thin flat disc, from which a highly-flattened 'Population I' stellar component is formed; in Model 1, on the other hand, a comparably-flattened disc is not formed because the higher viscosity causes the residual gas to spiral rapidly into the centre before it has had time to settle into a very thin disc. It is clear from these results that the relative prominence and flattening of a disc-like component depend not only on the initial angular velocity but also on the amount of viscosity present during the later stages of the collapse: a high viscosity tends to inhibit the formation of a thin disc, whereas a lower viscosity favours the formation of a disc, as is particularly evident in the inviscid model illustrated in Fig. 1.

Since the 'incipient disc' component of Model 4 forms during the later stages of the collapse from the relatively small amount of residual gas (≈ 5 per cent)

which is not used up in the formation of the spheroidal 'halo' component, the formation of such a disc could be suppressed by any process which might remove the gas from the system before star formation is complete. For galaxies of low or moderate mass, it seems possible that a significant amount of residual gas can be removed by supernova-driven winds (Larson 1974b), thus possibly suppressing the formation of any perceptible disc component. A galaxy may also have its residual gas swept out by its motion through a dense ambient intergalactic medium (Gisler 1975), again possibly suppressing the formation of a disc component.

Although the density contours shown in Fig. 8(a) qualitatively resemble the isophotes of some of the more flattened E galaxies, the departure from perfect ellipses is actually greater than is observed in the majority of E galaxies. The pointed structure of the model density contours seems instead to correspond more closely to the pointed isophotes of a number of So galaxies (van Houten 1961), so it may be that Model 4 should be considered as representing an So galaxy or a transition between E and So, rather than a typical E galaxy. Unfortunately, the classification of galaxies as E or So is based on subjective rather than quantitative criteria, so it is difficult to be more precise about the relation between models and galactic morphological classes. At any rate, the model results suggest that, depending on the details of the gas dynamics during the later stages of the collapse, it is possible to obtain a continuous sequence of galaxy types ranging from 'pure elliptical' systems with little or no disc component to So-like systems in which the presence of a disc component is quite evident.

The ellipticity profile of Model 4 is shown in Fig. 10(a), along with the profiles of two similar models calculated with different values of the parameter C_δ. The ellipticity profile of Model 4 differs qualitatively from those shown in Fig. 5 in that instead of being peaked, it is nearly flat at large radii and rises somewhat at small radii. The increase in $\epsilon(r)$ at small radii occurs because in Model 4 the viscosity decreases during the final stages of the collapse when the nucleus is being formed. Although this type of profile is less commonly observed than the type illustrated in Fig. 5, there are nevertheless some E galaxies whose ellipticity profiles decrease monotonically, or are concave upward like those shown in Fig. 10(a). Like the previous results, the profiles shown in Fig. 10(a) demonstrate that the ellipticity of the outer part of the system is not much affected by the assumed viscosity, whereas $\epsilon(r)$ in the inner regions is quite sensitive to the assumed viscosity.

4.5 *Effect of the assumed star formation rate*

Finally, we present some results for Model 5, in which the gaseous dissipation and star formation rates are assumed to be related to the local dynamical time scale via equations (1) and (3) of Paper II, with $C_D = C_S = 0.75$. The assumed initial velocity dispersion is $\alpha^{1/2} = 20\ \mathrm{km\ s^{-1}}$, and the initial angular velocity is $\omega_0 = 0.001\ 33\ (10^6\ \mathrm{yr})^{-1}$. Viscosity has been treated by using the Navier–Stokes equations, but instead of using a cloud model to evaluate the kinematic viscosity ν, we have used the relation $\nu \sim \alpha\tau$, where τ is the mean free time between collisions of the independently moving gas elements; we assume that τ, like the dissipation time, is proportional to the local free-fall time t_f, so that

$$\nu = C_\tau \alpha t_f \tag{20}$$

where C_τ is a dimensionless constant of order unity and t_f is given by equation (2)

of Paper II. In Model 5 we have assumed $C_\tau = 1{\cdot}0$. Only one such model has been calculated because of the large amount of computation required to follow the more violent motions generated during the collapse and approach to equilibrium of models of this type.

The distributions of stellar density and metal abundance found for Model 5 are shown in Fig. 9(a) and (b). The density distribution is similar to that of Model 1

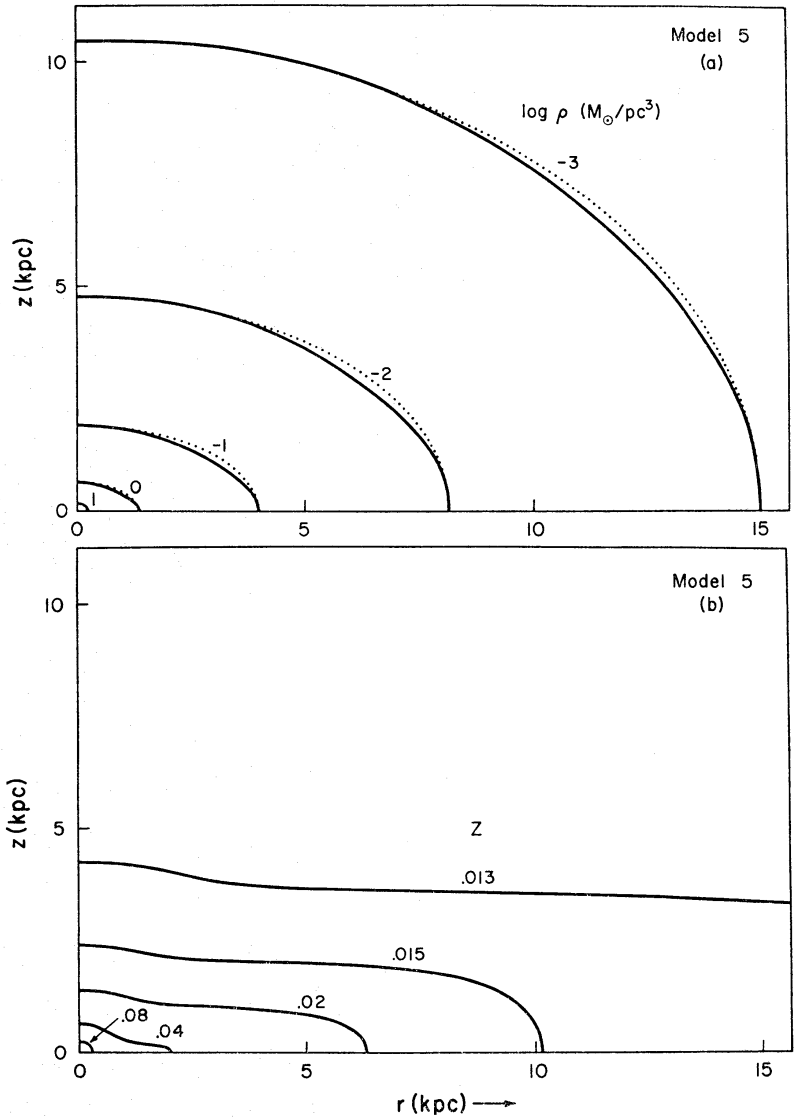

FIG. 9. (*a*) *Contours of equal stellar density for Model* 5. (*b*) *Contours of average stellar metal abundance for Model* 5.

(Fig. 2(a)), except for a somewhat higher ellipticity and lower density near the centre. The relatively low central density makes this model less realistic in detail than Models 1–4, and appears to be related to the fact that viscous redistribution of angular momentum is less effective during the early stages of the collapse than in the other models, so that there is less low angular momentum material to form a dense core. This presumably means that the particular combination of assumptions used here is not realistic in all details; however, we note that there do appear to be significant differences in the core densities of different elliptical

galaxies (Burbidge, Burbidge & Crampin 1964; King & Minkowski 1966). The ellipticity profile of Model 5 is shown in Fig. 10(b); it has a broad peaked structure similar to those shown in Fig. 5.

The metal abundance distribution of Model 5, shown in Fig. 9(b), is again strongly flattened toward the equatorial plane, but as in the corresponding spherical models the average stellar metal abundance remains fairly high and nearly constant in the halo region. Outside the contour $Z = 0{\cdot}013$ in Fig. 9(b), the metal abundance remains everywhere between 0·012 and 0·013. The relatively high metal abundance in the halo is due in this case, as in the corresponding spherical models, to the occurrence of relatively efficient star formation during the early stages of the collapse, producing substantial metal enrichment before there has been time for much separation between gas and stars. By contrast, the power law star formation rate of Models 1–4 predicts less efficient star formation and less metal production during the earliest stages of the collapse, and an inflow of gas relative to the stars begins at an early stage to establish a composition gradient.

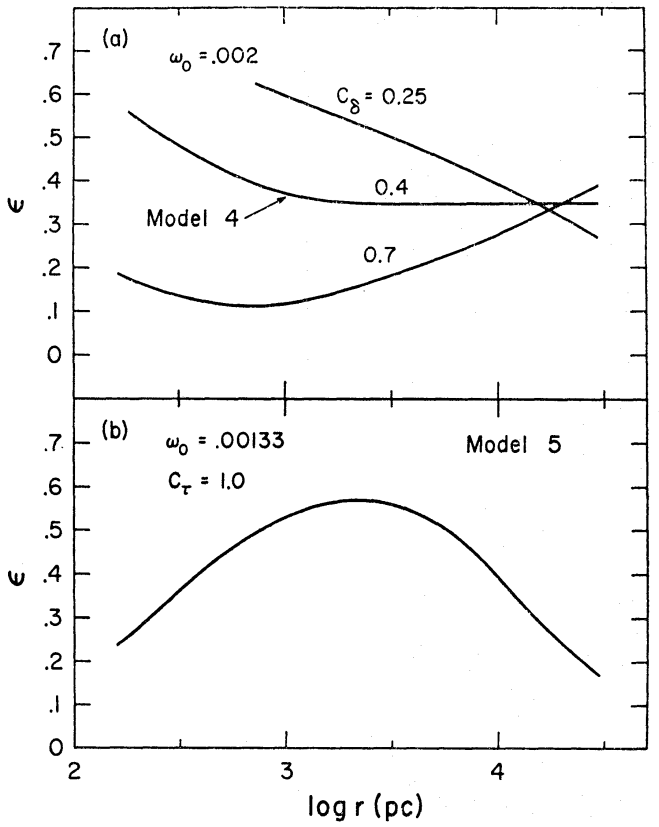

FIG. 10. (*a*) *Ellipticity profiles for* 3 *models calculated with the same assumptions as Model* 4 *but with different values of the viscosity parameter* C_δ. (*b*) *Ellipticity profile of Model* 5.

5. SUMMARY AND CONCLUSIONS

5.1 *Formation of spheroidal systems*

A principal conclusion of the present investigation is the necessity of including some form of outward transport of angular momentum in a collapsing protogalaxy if realistic models of elliptical galaxies are to be obtained. Such outward transfer

of angular momentum is expected to occur in any picture in which large random motions are present during the formation of a galaxy, and may be regarded as being due to a 'turbulent viscosity'. Gravitational torques associated with bar or spiral instabilities may also contribute to the outward transfer of angular momentum if part of the mass distribution becomes sufficiently flattened, but this effect is more difficult to estimate and has been neglected here. If the viscosity of the protogalactic gas is calculated using the same assumptions that were previously adopted in estimating the gaseous dissipation rate, models are obtained which closely resemble typical elliptical galacies in all respects, but comparable agreement is not obtained if the assumed viscosity is much smaller or larger. The necessity of including such a 'turbulent viscosity' effect provides additional support for the general concept that large inhomogeneities and random motions play an important role in collapsing protogalactic gas clouds.

The model calculations clearly demonstrate the sensitivity of the resulting ellipticity profile to the amount of viscous redistribution of angular momentum that takes place in a collapsing protogalaxy; if this is different in different protogalaxies, this might plausibly account for the observed differences in the ellipticity profiles of E galaxies. Such differences in the details of turbulent transfer of angular momentum would be especially important if each protogalaxy is built up of only a small number of independently moving gas elements or clouds. As an extreme example of this type of picture, we note the suggestion by Toomre (1974, 1975) that some E galaxies may have formed as a result of collisions and mergers between smaller galaxies. While it still seems necessary to invoke infall of residual gas to account for the metal abundance gradients and dense nuclei of E galaxies, it is not implausible that collisions could have played a role in the early stages of formation of E galaxies, perhaps at a time when the colliding systems were still mostly gaseous. If so, the elliptical galaxies may not be as simple and homogeneous a class of objects as has usually been supposed.

The radial structure and evolution of the present models are generally similar to those of the spherical models previously studied in Papers I and II, and are not greatly altered by the presence of rotation provided that viscosity is included as described above. Thus the conclusions of Paper II concerning the time evolution of forming galaxies, the production of metal abundance gradients, and the formation of dense nuclei and the possible relation of this to nuclear activity, are still qualitatively valid for the present rotating models. Also, the conclusions of Larson & Tinsley (1974) concerning the photometric properties, and the conclusions of Larson (1974b) about the importance of early gas loss in galaxies of small mass, will still apply without major modification in the rotating case. The main difference concerns the later evolution of the gas and young stellar content, if any, in an elliptical galaxy: in the rotating case a significant part of the residual gas does not fall to the centre but remains relatively widely distributed in a flattened disc-like configuration, within which star formation proceeds relatively slowly. Possibly this would make supernova-driven gas loss (Mathews & Baker 1971; Larson 1974b) less efficient than if the star formation and supernova activity were more spherically distributed (see also Faber & Gallagher 1975). At any rate, if conditions are quiescent and gas loss is not important, the presence of gas and young stars near the equatorial plane would continue to be detectable in the rotating models for at least several times 10^9 yr.

All of the rotating models possess to some degree a composite structure, and

may be described as being made up of a sequence of stellar populations with increasing flattening, increasing rotational velocity, decreasing velocity dispersion, and increasing metal abundance. This population sequence is also a chronological sequence, and directly reflects the collapse of the protogalactic gas cloud from an extended, nearly spherical, slowly rotating configuration toward a relatively flattened, rapidly rotating disc with a small velocity dispersion and a high metal abundance. The presence of a population gradient perpendicular to the equatorial plane is manifested in the deviation of the predicted density contours from perfect ellipses, but is even more strikingly evident in the predicted strong vertical gradients of metal abundance, rotational velocity, and velocity dispersion. All of these properties of the models agree qualitatively with the well-known characteristics of the stellar populations in our galaxy, but it is noteworthy that the models predict that similar, if less marked, population gradients should be present even in much less flattened elliptical galaxies. Observations to look for the predicted flattening of both the metal abundance distribution and, if possible, the distribution of kinematic properties in E galaxies would clearly be of great value in testing the validity of the present models and, more generally, of the entire picture of galaxy formation by a gaseous condensation process.

5.2 *Formation of disc systems*

We have seen that if there is not too much viscosity present during the later stages of the collapse and if the residual gas is not somehow removed from the system, the residual gas settles into and remains in a thin equilibrium disc, from which a stellar disc component is formed. Thus there is no difficulty in understanding, at least in principle, how the same qualitative collapse picture that explains the formation of elliptical galaxies might also account for the formation of the disc components of spiral and So galaxies. However, none of the models calculated with the simple assumptions described in this paper yielded a disc component much more prominent than that of Model 4, i.e. one containing more than about 5–10 per cent of the total mass. The failure of the models to produce more massive disc components is due simply to the fact that in order to explain the formation of *elliptical* galaxies, star formation must be reasonably efficient during the collapse of a protogalaxy, so that most of the gas is transformed into stars before it has had time to settle to a disc. If the star formation rate were much lower, the gas might collapse to a much flatter disc-like configuration before forming star, but this would still not explain the formation of galaxies in which both disc and halo components are present in varying proportions. What appears to be required is a more complicated two-stage formation process in which the first stage produces a spheroidal halo, as in the present models, and the second stage involves continuing infall of leftover gas with much less efficient star formation, so that most of this gas settles into a thin disc before forming stars.

It is not implausible that star formation would become much less efficient during the later stages of formation of a galaxy, after a halo of significant mass has already formed and residual gas of lower density is continuing to fall inward through it. This residual gas may be relatively hot as a result of heating by hot stars, supernovae, etc., and it will also be subject to strong tidal forces which will tend to prevent local collapse to form stars until the gas has settled into a thin dense disc. Depending on how much leftover gas continues to fall into the

system after the formation of a halo, it would seem possible in this way to account for the formation of galaxies with almost any ratio of disc mass to halo mass. A possibly promising scenario for the formation of spiral galaxies (Larson 1975) might then involve the formation first of spheroidal halos by the rapid collapse of relatively dense condensations in the pre-galactic medium, followed by the infall of varying amounts of lower-density ambient gas to form discs. Thus, while the formation of spheroidal systems would be expected to occur relatively rapidly, the formation of disc systems could take a much longer time, and it is even possible that the slow infall or settling down of residual gas to form a flat disc could continue for 10^{10} yr or longer (Larson 1972a; Paper II). Perhaps many of the observed irregularities in the distribution and dynamics of the gas in the outer parts of spiral galaxies, including such phenomena as ' warps ', ' extensions ', and large scale non-circular motions, may reflect such slow settling of outlying gas into the fundamental plane of the galaxy.

REFERENCES

Bertola, F. & Capaccioli, M., 1975. In press.
Burbidge, E. M., Burbidge, G. R. & Crampin, D. J., 1964. *Astrophys. J.*, **140,** 1462.
Burkhead, M. S. & Kalinowski, J. K., 1974. *Astr. J.*, **79,** 835.
de Vaucouleurs, G., 1959. *Handbuch der Physik* **53,** *Stellar systems*, p. 311, ed. S. Flügge, Springer-Verlag, Berlin.
de Vaucouleurs, G., 1974. *The formation and dynamics of galaxies, IAU Symp. No. 58*, p. 1, ed. J. R. Shakeshaft, D. Reidel, Dordrecht.
Faber, S. M. & Gallagher, J. S., 1975. *Astrophys. J.*, in press.
Gisler, G. R., 1975. *Astr. Astrophys.*, in press.
Gott, J. R., 1973. *Astrophys. J.*, **186,** 481.
Gott, J. R., 1975. *Astrophys. J.*, in press.
Hohl, F., 1971. *Astrophys. J.*, **168,** 343.
King, I. R. & Minkowski, R., 1966. *Astrophys. J.*, **143,** 1002.
King, I. R., 1975. In preparation.
Landau, L. D. & Lifschitz, E. M., 1959. *Fluid mechanics*, Pergamon Press Ltd, London.
Larson, R. B., 1969. *Mon. Not. R. astr. Soc.*, **145,** 405 (Paper I).
Larson, R. B., 1970. *Mon. Not. R. astr. Soc.*, **147,** 323.
Larson, R. B., 1972a. *Nature*, **236,** 21.
Larson, R. B., 1972b. *Mon. Not. R. astr. Soc.*, **156,** 437.
Larson, R. B., 1974a. *Mon. Not. R. astr. Soc.*, **166,** 585 (Paper II).
Larson, R. B., 1974b. *Mon. Not. R. astr. Soc.*, **169,** 229.
Larson, R. B., 1975. *Dynamics of stellar systems, IAU Symp. No. 69*, p. 247, ed. A. Hayli, D. Reidel, Dordrecht.
Larson, R. B. & Tinsley, B. M., 1974. *Astrophys. J.*, **192,** 293.
Liller, M. H., 1960. *Astrophys. J.*, **132,** 306.
Liller, M. H., 1966. *Astrophys. J.*, **146,** 28.
Mathews, W. G. & Baker, J. C., 1971. *Astrophys. J.*, **170,** 241.
McCrea, W. H., 1960. *Proc. R. Soc.*, **A256,** 245.
Morton, D. C. & Chevalier, R. A., 1973. *Astrophys. J.*, **179,** 55.
Rood, H. J. & Baum, W. A., 1968. *Astr. J.*, **73,** 442.
Spinrad, H., Smith, H. E. & Taylor, B. J., 1972. *Astrophys. J.*, **175,** 649.
Toomre, A., 1974. *The formation and dynamics of galaxies, IAU Symp. No. 58*, p. 347, ed. J. R. Shakeshaft, D. Reidel, Dordrecht.
Toomre, A., 1975. In preparation.
van Houten, C. J., 1961. *Bull. astr. Inst. Netherl.*, **16,** 1.
Wilson, C. P., 1975. *Astr. J.*, **80,** 175.

APPENDIX

ANGULAR MOMENTUM TRANSFER IN PROTOGALAXIES

In this Appendix we discuss approximate solutions of the hydrodynamic moment equations governing a rotating and self-gravitating system of particles. To simplify the analysis while retaining the essential qualitative aspects of the problem, we assume cylindrical symmetry; we then have a single space coordinate r, i.e. the distance from the axis of rotation, and two velocity components, u and w, in the radial and transverse directions respectively. The state of the system at any time t is specified by the distribution function $f(r, u, w, t)$, which gives the density of particles in a 3-dimensional phase space with coordinates r, u, w. The time dependence of f is governed by the Boltzmann equation, which in the case of cylindrical symmetry takes the form

$$\frac{\partial f}{\partial t}+u\frac{\partial f}{\partial r}+\left(\frac{w^2}{r}-\frac{\partial \Phi}{\partial r}\right)\frac{\partial f}{\partial u}-\frac{uw}{r}\frac{\partial f}{\partial w}=\left(\frac{\partial f}{\partial t}\right)_c \tag{A1}$$

where $\Phi(r, t)$ is the gravitational potential and $(\partial f/\partial t)_c$ represents the effect of particle collisions on f.

In addition to the usual zero- and first-order moments ρ, $\langle u\rangle$, and $\langle w\rangle$, it is necessary in order to provide an adequate description of viscosity effects to define the following second-order moments of the velocity distribution:

$$\begin{aligned}\alpha &= \langle(u-\langle u\rangle)^2\rangle\\ \beta &= \langle(w-\langle w\rangle)^2\rangle\\ \delta &= \langle(u-\langle u\rangle)(w-\langle w\rangle)\rangle.\end{aligned} \tag{A2}$$

The moment δ is the crucial quantity describing the radial transfer of angular momentum by random motions; a positive value of δ, for example, means that particles with $u-\langle u\rangle > 0$ preferentially have $w-\langle w\rangle > 0$, so that there is a net outward transfer of angular momentum. It is essential to treat α and β separately because in general $\alpha \neq \beta$, and the difference between α and β is closely coupled to the magnitude and sign of the viscosity. However, it appears that the various third-order moments arising in the derivation of the moment equations do not play any essential role in the viscous transfer of angular momentum and may be neglected without destroying the qualitative validity of the equations. The neglect of the third-order moments is also weakly justified by previous experience with the use of higher moments (Larson 1970) which suggests that the third-order moments are generally small and play an important role only in the relatively slow evolution caused by two-body relaxation processes. We then obtain from the Boltzmann equation the following set of moment equations complete through second order:

$$\frac{\partial \rho}{\partial t}+\frac{1}{r}\frac{\partial}{\partial r}r\rho\langle u\rangle = 0 \tag{A3}$$

$$\frac{\partial\langle u\rangle}{\partial r}+\langle u\rangle\frac{\partial\langle u\rangle}{\partial r}+\frac{1}{\rho}\frac{\partial}{\partial r}\rho\alpha-\frac{\langle w\rangle^2}{r}+\frac{(\alpha-\beta)}{r}+\frac{\partial\Phi}{\partial r} = 0 \tag{A4}$$

$$\frac{\partial\langle w\rangle}{\partial t}+\frac{\langle u\rangle}{r}\frac{\partial}{\partial r}r\langle w\rangle+\frac{1}{r^2\rho}\frac{\partial}{\partial r}r^2\rho\delta = 0 \tag{A5}$$

$$\frac{\partial\alpha}{\partial t}+\langle u\rangle\frac{\partial\alpha}{\partial r}+2\alpha\frac{\partial\langle u\rangle}{\partial r}-\frac{4\langle w\rangle\delta}{r}=\left(\frac{\partial\alpha}{\partial t}\right)_c \tag{A6}$$

$$\frac{\partial\beta}{\partial t}+\langle u\rangle\frac{\partial\beta}{\partial r}+2\beta\frac{\langle u\rangle}{r}+\frac{2\delta}{r}\frac{\partial}{\partial r}r\langle w\rangle=\left(\frac{\partial\beta}{\partial t}\right)_c \tag{A7}$$

$$\frac{\partial\delta}{\partial t}+\langle u\rangle\frac{\partial\delta}{\partial r}+\frac{\delta}{r}\frac{\partial}{\partial r}r\langle u\rangle+\left[\frac{\alpha}{r}\frac{\partial}{\partial r}r\langle w\rangle-\frac{2\beta\langle w\rangle}{r}\right]=\left(\frac{\partial\delta}{\partial t}\right)_c. \tag{A8}$$

The effect of particle collisions and finite mean free paths is represented by the collision terms $(\partial\alpha/\partial t)_c$, etc., on the right-hand sides of equations (A6)–(A8). To obtain an approximate solution for the viscosity moment δ, we consider first the limit of very small mean free paths; the velocity distribution is then nearly Maxwellian, so that α is nearly equal to β and δ is very small. We can then neglect the first three terms on the left-hand side of equation (A8) and set $\alpha=\beta$ in the remaining terms; equation (A8) then reduces to

$$\alpha\left(\frac{1}{r}\frac{\partial}{\partial r}r\langle w\rangle-\frac{2\langle w\rangle}{r}\right)=\left(\frac{\partial\delta}{\partial t}\right)_c$$

or

$$\alpha r\frac{\partial}{\partial r}\frac{\langle w\rangle}{r}=-\frac{\delta}{\tau}, \tag{A9}$$

where τ is the relaxation time for decay of δ due to particle collisions, and is approximately equal to the mean free time between collisions. Equation (A9) shows that in the limit of small mean free paths and a nearly Maxwellian velocity distribution the viscous stress is proportional to the gradient of the angular velocity $\langle w\rangle/r$, i.e. to the local shear of the velocity field. This equation can be rewritten slightly as

$$\delta=-\nu r\frac{\partial}{\partial r}\frac{\langle w\rangle}{r} \tag{A10}$$

where ν is the kinematic viscosity as usually defined, and as given by equation (1). If we substitute equation (A10) into equation (A5), we arrive at the classical Navier–Stokes equation for the rotational velocity of a viscous gas in the case of cylindrical symmetry.

In the opposite limit of very long mean free paths or collisionless dynamics, the right-hand sides of equations (A6)–(A8) vanish and it is no longer possible to obtain a simple approximate solution for δ as above. However, it is instructive to consider the special case of an equilibrium system, e.g. an equilibrium stellar disc, in which all time derivatives, as well as $\langle u\rangle$ and δ, must vanish. From equation (A8) we see that this can be the case only if the quantity in square brackets vanishes, i.e. if

$$\frac{\alpha}{r}\frac{\partial}{\partial r}r\langle w\rangle-\frac{2\beta\langle w\rangle}{r}=0. \tag{A11}$$

This relation is familiar in galactic dynamics in the form

$$\frac{\beta}{\alpha}=\frac{-B}{A-B},$$

where A and B are the Oort constants, defined in the usual way in terms of $\langle w\rangle/r$ and $\partial\langle w\rangle/\partial r$. If equation (A11) is not satisfied, we see from equation (A8) that δ cannot remain equal to zero, so there must occur a viscous transfer of angular

momentum whose magnitude and sign depend on the magnitude and sign of the quantity in square brackets, and hence on the degree of anisotropy of the velocity distribution. In this situation the Navier–Stokes equations are clearly not applicable, and may even give the wrong sign for the viscosity effect.

Without solving the complete set of moment equations, it is still possible to determine the sign of δ during the early stages of the collapse of a system of particles. We assume that the system begins with pure uniform rotation and an isotropic velocity distribution, so that initially $\langle u \rangle = 0$, $\langle w \rangle \propto r$, $\alpha = \beta$, and $\delta = 0$. For any nonhomologous collapse, we in general have $\partial \langle u \rangle / \partial r > \langle u \rangle / r$; equations (A6) and (A7) then imply that $\delta\alpha/\partial t < \partial\beta/\partial t$, and hence that $\alpha < \beta$ during the early stages of the collapse. A non-homologous collapse also produces differential rotation with $\partial(r\langle w \rangle)/\partial r < 2\langle w \rangle$; the quantity in square brackets in equation (A8) is then negative, implying that $\partial\delta/\partial t > 0$ and hence that $\delta > 0$ during at least the early stages of the collapse. We therefore predict that angular momentum is transferred outward, even if the mean free paths are long and the Navier–Stokes equations are not applicable.

To find a simple dimensional expression for δ which predicts qualitatively the correct behaviour, we note from equation (A8) that δ is coupled to the rotational velocity $\langle w \rangle$ and that, other things being equal, δ is proportional to the scale of $\langle w \rangle$: this suggests that we assume that δ is in general approximately proportional to $\langle w \rangle$. Equations (A6) and (A7) show that δ is also coupled to $\langle u \rangle$, albeit in a more complicated way; however, since we expect δ to vary roughly together with $\langle u \rangle$, being small initially when $\langle u \rangle$ is small, large when the collapse is proceeding rapidly, and small again when the gas settles into a flattened equilibrium configuration, we shall consider the assumption that δ is also approximately proportional to $-\langle u \rangle$. We then have the approximate relation

$$\delta \underset{\sim}{\propto} -\langle u \rangle \langle w \rangle \tag{A12}$$

which implies, as mentioned in Section 2.3, the not unreasonable result that the rate of outward transfer of angular momentum by random motions is proportional to the rate of inward transfer of angular momentum by the mean flow. For purposes of calculation we have assumed that

$$\delta = -C_\delta \langle u \rangle \langle w \rangle, \tag{A13}$$

where the dimensionless constant C_δ has been treated as a free parameter. We expect that C_δ is of order unity but perhaps somewhat smaller than unity; values ranging from 0·25 to 0·7 have been tried in the model calculations.

We must finally generalize the above approximations to the case of an axisymmetric system described by spherical polar coordinates r, θ, ϕ and the corresponding velocity components u, v, w. The equation for $\langle w \rangle$ which takes the place of equation (A5) has already been given as equation (9), and the moments δ_r and δ_θ are defined by equations (11). In the limit of short mean free paths, in which the viscous stress is proportional to the local shear of the velocity field, we have

$$\left.\begin{aligned} \delta_r &= -\nu r \frac{\partial}{\partial r} \frac{\langle w \rangle}{r} \\ \partial_\theta &= -\nu \frac{\sin\theta}{r} \frac{\partial}{\partial\theta} \frac{\langle w \rangle}{\sin\theta} \end{aligned}\right\} \tag{A14}$$

(e.g. Landau & Lifschitz 1959; equation (15.17)). Substitution of equations (A14) into equation (9) then yields the Navier–Stokes equation for $\langle w \rangle$ in spherical coordinates for an axisymmetric system. (This equation becomes identical to the third of equations (15.18) of Landau & Litschitz (1959) in the special case where ρ and ν are spatially uniform.)

The generalization of the alternative expression (A13) for the viscosity moment δ requires a further assumption to allow the evaluation of both δ_r and δ_θ. We have simply assumed that, as in the case of cylindrical symmetry, angular momentum is transferred only in the direction perpendicular to the rotation axis, and at a rate proportional to the component of velocity in this direction. In other words, we neglect any viscous transfer of angular momentum parallel to the rotation axis. Then we have

$$\left.\begin{aligned} \delta_r &= -C_\delta (\langle u \rangle \sin\theta + \langle v \rangle \cos\theta) \langle w \rangle \sin\theta \\ \delta_\theta &= -C_\delta (\langle u \rangle \sin\theta + \langle v \rangle \cos\theta) \langle w \rangle \cos\theta. \end{aligned}\right\} \quad \text{(A15)}$$

Substitution of these expressions into equation (9) again leads to a closed system of hydrodynamic equations which can be solved as before to calculate the dynamical evolution of the system.